AIAA JOURNAL
Vol. 42, No. 1, January 2004

Core and Face-Sheet Anisotropy in Deformation and Buckling of Sandwich Panels

Jörg Hohe*
Fraunhofer Institut für Werkstoffmechanik, 79108 Freiburg/Breisgau, Germany
and
Liviu Librescu†
Virginia Polytechnic Institute and State University, Blacksburg, Virginia 24061

A theoretical study of the effects of face sheets anisotropy and of the transverse compressibility of the core on buckling and deformation of sandwich flat/curved panels is presented. Additionally, the effect of core orthotropy is addressed. The analysis is carried out in the context of a newly geometrically nonlinear higher-order sandwich shell model developed by the authors. An analytical solution is obtained by means of an extended Galerkin procedure. Both the overall buckling mode and the local face wrinkling instability mode are addressed. It is observed that the global and local instabilities are coupled rather than being independent features. Furthermore, the face wrinkling instability might have a considerable effect on the overall deformation behavior of the structure in the (global) prebuckling range. Both the stacking sequence of the face sheets and the orthotropicity of the core are found to have a significant effect on the occurrence of the different instability modes.

Nomenclature

A_{ij}, D_{ij}, F_{ij}, H_{ij}	=	stiffness components
E_{ij}, G_{ij}, ν_{ij}	=	anisotropic elasticity constants
l_i	=	panel edge lengths
M_{ij}, N_{ij}	=	stress couples and stress resultants
m, n, p, q	=	number of sine half waves for the different stability modes
Q_{ij}	=	reduced stiffness matrix
q_i	=	transverse pressure loads
r_i	=	radii of curvature
T	=	kinetic energy
t	=	layer thicknesses
U	=	strain energy
u_i, $\mathring{u}_i$	=	shell midplane displacements and initial geometric imperfection
v_i	=	three-dimensional shell displacements
W	=	work done by external loads
w, $\mathring{w}$	=	modal amplitude of transverse displacement and initial geometric imperfection
x_i	=	Gaussian orthogonal coordinate system
γ_{ij}	=	Green–Lagrange strain tensor
$\bar{\gamma}_{ij}$, κ_{ij}	=	two-dimensional strain component measures
$\delta(\ldots)$	=	variation of a quantity
ϵ_{ij}	=	permutation symbol
λ, μ	=	wavelength parameters
ρ	=	mass density
τ_{ij}	=	second Piola–Kirchhoff stress tensor
Φ	=	Airy stress function
Ω_i	=	higher-order displacement functions

Superscripts

a	=	average of quantities related to the top and bottom face sheet
b	=	quantities related to the bottom face sheet
c	=	quantities related to the core
d	=	half difference of quantities related to the top and bottom face sheet
t	=	quantities related to the top face sheet
$\hat{}$	=	prescribed quantity
$\ddot{}$	=	second derivative with respect to time

I. Introduction

STRUCTURAL sandwich panels are important elements in modern lightweight construction. The principle of sandwich construction is well established in all fields of aerospace technology. Nowadays, sandwich panels today can be found in many other technological fields such as in high-speed ferries, high-speed passenger trains, or automotive applications. Especially in the naval industry, there is a strong trend to use sandwich shells in the construction of ship hulls. Other innovative examples include civil engineering structures, such as highway bridge decks.

The typical structural sandwich panel consists of three principal layers, where two high-density face sheets are adhesively bonded to a low-density cellular core (Fig. 1). In most cases, the core is made from a two-dimensional cellular structure or a foamed material, whereas composite laminas are common face-sheet materials. Within the principle of sandwich construction, the face sheets carry the tangential and bending loads, whereas the core keeps the face sheets at their desired distance and transmits the transverse normal and shear loads. Both the core and the face-sheet layers are in general anisotropic.

Because of the presence of the thick core layer made from a weak material, the deformation and buckling behaviors of structural sandwich panels are essentially different from the deformation and buckling behaviors of standard laminated or monolayer structures. Beside the standard overall buckling, the transverse compressibility of the core enables the development of an additional local instability mode referred to as face-wrinkling instability. Within this type of instability, the face sheets buckle into the core region, whereas the entire structure might remain globally stable.

To account for the specific deformation behavior of sandwich structures, different types of models have been developed. These can be classified into effective single-layer approaches using a single

Received 14 March 2003; presented as Paper 2003-1928 at the AIAA/ASME/ASCE/AHS 44th Structures, Structural Dynamics, and Materials Conference, Norfolk, VA, 7–10 April 2003; revision received 2 August 2003; accepted for publication 5 August 2003.

*Scientist, Fraunhofer Institut für Werkstoffmechanik, Wöhlerstr. 11; hohe@iwm.fhg.de.

†Professor, Department of Engineering Science and Mechanics; librescu@vt.edu.

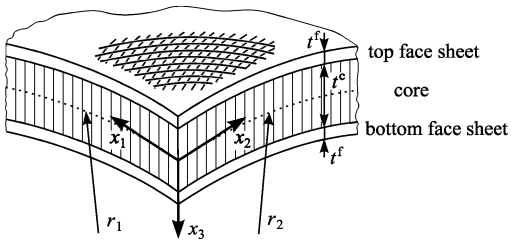

Fig. 1 Structural sandwich panel.

displacement function for all layers and multilayer models, which treat the three principal layers independently and apply appropriate continuity conditions at the interfaces between the face sheets and the core.

Recent effective single-layer models have been presented in papers by Skvortsov and Bozhevolnaya,[1] as well as by Ferreira et al.[2] The first study is directed to linear elastic material behavior, whereas the latter one accounts for geometric and material nonlinearities. An innovative approach based on weighted average displacement functions in conjunction with a continuous stress field at the interfaces has been presented by Barut et al.[3]

Examples for multilayer models include the early sandwich membrane models for the face sheets, for example, Allen,[4] as well as a number of more sophisticated approaches. In this context, the geometrically linear sandwich beam model by Frostig et al.[5] has to be mentioned. This model is based on a mixed formulation where the Kirchhoff–Love hypothesis is adopted for the face sheets, whereas an assumed stress field is used to describe the core behavior. This approach has later been extended to curved sandwich beams by Bozhevolnaya and Frostig,[6] as well as to plane sandwich plates by Frostig.[7] Alternative models have recently been presented by Dawe and Yuan[8] and Yuan and Dawe,[9] as well as by Pai and Palazotto.[10] A general von Kármán-type theory for doubly curved sandwich shells with transversely incompressible core has been presented by Librescu et al.[11] Vonach and Rammerstorfer[12] provided a general local model to address the face-wrinkling instability in orthotropic sandwich plates independently from the overall deformation. Surveys on recent work have been provided by Librescu and Hause,[13] Noor et al.,[14] and Vinson.[15]

It has been pointed out both by Frostig et al.[5] and Starlinger and Rammerstorfer[16] that the transverse core compressibility that induces the face-wrinkling instability should be considered during the structural analysis of the entire sandwich shell because, due to the geometrically nonlinear nature of the buckling phenomenon, both types of instability are coupled rather than independent features. Especially if the buckling loads for both instability types are in the same order of magnitude, strong interaction effects have to be expected. Coupling effects between the local and the global instability have independently been reported by da Silva and Santos[17] and by Wadee and Hunt.[18] Because of these coupling effects, the standard sandwich sandwich model postulating the incompressibility of the core is not likely to provide accurate predictions for the face-wrinkling instability. Thus, an enhanced structural model accounting for the transverse compressibility of the core is required.

The present study is concerned, among other issues, with anisotropy effects on both the global buckling and the local face-wrinkling instabilities. For the analysis, a general, geometrically nonlinear model for doubly curved sandwich shells is utilized. The model adopts the standard Kirchhoff model for the face sheets, whereas a first- and second-order displacement expansion is used for the core layer. Additional features include the effect of initial geometric imperfections and inertia effects. Consistent equations of motion and the corresponding boundary conditions are derived by means of Hamilton's principle. An analytical solution is obtained by means of an extended Galerkin procedure, for example, see Hohe and Librescu.[19,20] In comparison to experimental and other theoretical and numerical approaches, the present model proves to be both accurate and efficient. Subsequently, the model is applied to the analysis of different cases of sandwich shells. Strong implications of core and face-sheet anisotropy on both the global and the local instabilities are observed. Furthermore, it is found that the development of the local face-wrinkling instability has, in general, strong effects on the overall load deflection behavior as well.

II. Higher-Order Sandwich Shell Model

A. Basic Assumptions

The present study is based on a higher-order sandwich shell model. The model has been developed in a recent paper by the present authors. To be reasonably self-contained, a brief outline of this structural model and the analytical solution procedure is presented in Secs. II and III, respectively. Full details are given in the original paper.[20]

Consider a sandwich shell as presented in Fig. 1. The shell is symmetric with respect to the global midsurface, used subsequently as the shell reference surface. The thickness t^f of the top and bottom face sheets is assumed to be equal and uniform throughout the entire structure. The core thickness t^c is also uniform but larger than the face-sheet thickness t^f. The radii of curvature r_1 and r_2 of the midsurface are assumed to be much larger than the panel thickness so that the assumptions of shallow shell theory can be applied. For the analysis, an orthogonal Gaussian coordinate system is defined, where x_1 and x_2 are the tangential directions, whereas x_3 is the transverse downward normal direction.

The geometical nonlinearity of the structural response is included in the von Kármán sense. Thus, a sandwich shell model featuring large deflections and small strains is derived. Only the transverse lateral inertia effects will be considered, whereas the tangential as well as all rotatory inertia terms are neglected. The effect of an initial geometric imperfection will be included, which is also required for regularization of the bifurcation behavior in postbuckling analyses. In the basic form of the shell model, no specific constitutive behavior will be adopted. Subsequently, the special case of linear orthotropic elasticity will be considered.

B. Kinematic Relations

The three-dimensional mechanical behavior of the sandwich panel has to be projected onto the shell reference surface. Therfore, the three-dimensional displacements $v_i^t(x_j)$, $v_i^b(x_j)$, and $v_i^c(x_j)$ of the top face sheet, the bottom face sheet, and the core, respectively, are expanded into power series with respect to the transverse direction x_3.

Because the face sheets are thin, linear variation of the tangential displacements and uniformity of the transverse displacements with respect to the transverse direction x_3 need to be considered. Thus, the standard Kirchhoff–Love hypotheses applies to the face sheets. The following equations are obtained for the three-dimensional displacements v_i^t and v_i^b of the top and bottom face sheets in terms of the two-dimensional displacement measures u_i^a and u_i^d:

$$v_1^t = u_1^a + u_1^d - [x_3 + (t^c + t^f)/2]u_{3,1}^a - [x_3 + (t^c + t^f)/2]u_{3,1}^d \quad (1)$$

$$v_2^t = u_2^a + u_2^d - [x_3 + (t^c + t^f)/2]u_{3,2}^a - [x_3 + (t^c + t^f)/2]u_{3,2}^d \quad (2)$$

$$v_3^t = u_3^a + u_3^d \quad (3)$$

$$v_1^b = u_1^a - u_1^d - [x_3 - (t^c + t^f)/2]u_{3,1}^a + [x_3 - (t^c + t^f)/2]u_{3,1}^d \quad (4)$$

$$v_2^b = u_2^a - u_2^d - [x_3 - (t^c + t^f)/2]u_{3,2}^a + [x_3 - (t^c + t^f)/2]u_{3,2}^d \quad (5)$$

$$v_3^b = u_3^a - u_3^d \quad (6)$$

In these equations, the generalized two-dimensional displacement functions u_i^a and u_i^d are defined by

$$\left\{u_i^a, u_i^d\right\} = \tfrac{1}{2}\left\{\left(u_i^t + u_i^b\right), \left(u_i^t - u_i^b\right)\right\} \quad (7)$$

where u_i^t and u_i^b are the midsurface displacements of the top and bottom face sheets, respectively. It is implicitly understood that the

displacement functions $u^t(x_\alpha)$ and $u^b(x_\alpha)$ do not depend on the transverse direction x_3 ($\alpha = 1, 2$).

For the core layer, due to its large thickness, a higher-order power-series expansion has to be used. To include the transverse compressibility of the core, the representation of the transverse displacement has to be at least of first order with respect to the thickness coordinate x_3. In this case, a second-order expansion is appropriate for the tangential displacements. If the midsurface displacements u_3^c and their gradients $u_{3,\alpha}^c$ are eliminated by means of the displacement compatibility conditions with the face-sheet displacements at the interfaces at $x_3 = \pm t^c/2$, the power-series expansion of the core reads

$$v_1^c = u_1^a - (t^f/2)u_{3,1}^d - \left(2x_3/t^c\right)u_1^d + (t^f/t^c)x_3u_{3,1}^a + \left[4(x_3)^2/(t^c)^2 - 1\right]\Omega_1^c \tag{8}$$

$$v_2^c = u_2^a - (t^f/2)u_{3,2}^d - \left(2x_3/t^c\right)u_2^d + (t^f/t^c)x_3u_{3,2}^a + \left[4(x_3)^2/(t^c)^2 - 1\right]\Omega_2^c \tag{9}$$

$$v_3^c = u_3^a - \left(2x_3/t^c\right)u_3^d \tag{10}$$

where Ω_α^c are additional independent displacement functions that are related to the warping of the core layer.

In addition to the load-dependent displacements v_i^t, v_i^b, and v_i^c, initial geometric imperfections with respect to the transverse direction are included. These are defined as

$$\mathring{v}_3^t = \mathring{u}_3^a + \mathring{u}_3^d \tag{11}$$

$$\mathring{v}_3^b = \mathring{u}_3^a - \mathring{u}_3^d \tag{12}$$

$$\mathring{v}_3^c = \mathring{u}_3^a - \left(2x_3/t^c\right)\mathring{u}_3^d \tag{13}$$

The imperfections are assumed infinitesimal and constant during the loading and deformation process.

Because geometrically nonlinear theory is to be used in the present analysis, the deformation of the individual layers is described in terms of the Green–Lagrange strain tensor terms of the components

$$\gamma_{ij} = \tfrac{1}{2}(v_{i|j} + v_{j|i} + v_{k|i}v_{k|j}) \tag{14}$$

where the vertical stroke denotes the covariant derivative. The total displacements entering the strain–displacement relations are given by the sum of the load dependent displacements and the initial geometric imperfections. According to the von Kármán nonlinear concept, the strain–displacement relations (14) are not used directly, but all quadratic terms containing exclusively gradients of the tangential displacements are neglected. Further simplifications are due to the adoption of the assumtions $r_\alpha \gg t^c, t^f$ of shallow shell theory.

Substituting the displacement representations (1–10) of the face sheets and the core, as well as the initial geometric imperfection equations (11–13) into the resulting equations yields the expressions of the strain components γ_{ij} for both the face sheets and the core layer. When the assumption that no antisymmetric terms should occur in the expressions for the transverse shear stresses and strains is adopted, the equations for γ_{23} and γ_{13} yield explicit expressions for the core warping functions Ω_α^c. By substitution of the obtained expressions into the kinematic relations, the field variables Ω_α can be eliminated from the system. Because the expressions for the Green–Lagrange strain tensor components γ_{ij} are rather lengthy, the resulting expressions are not presented in explicit form.

C. Equations of Motion and Boundary Conditions

In Sec. II.B the three-dimensional displacements $v_i(x_k)$ for the individual layers and the corresponding nonlinear strain components $\gamma_{ij}(x_k)$ have been determined in terms of the midsurface displacements $u_i^a(x_\alpha)$ and $u_i^d(x_\alpha)$ of the face sheets as well as the warping $\Omega_\alpha^c(x_\alpha)$ of the core. Next, the corresponding nonlinear equations of motion and the corresponding boundary conditions have to be determined. In this context, to obtain a consistent theory, care has to be exercised to introduce similar simplifications as in the derivation of the strain–displacement relations.

A natural manner to derive a consistent structural model is the use of Hamilton's principle

$$\int_{t^0}^{t^1} (\delta U - \delta W - \delta T)\,\mathrm{d}t = 0 \tag{15}$$

where δU, δW, and δT are the variation of the strain energy, of the work done by the external loads, and of the kinetic energy, respectively, whereas t^0 and t^1 are arbitrary instants of time.

Consistent with the concept of soft core and in light of the earlier postulated assumptions, the variation of the strain energy is given by

$$\delta U = \int_A \left(\int_{-t^f - t^c/2}^{-t^c/2} \tau_{\alpha\beta}^t \delta\gamma_{\alpha\beta}^t\,\mathrm{d}x_3 + \int_{-t^c/2}^{t^c/2} \tau_{i3}^c \delta\gamma_{i3}^c\,\mathrm{d}x_3 + \int_{t^c/2}^{t^c/2+t^f} \tau_{\alpha\beta}^b \delta\gamma_{\alpha\beta}^b\,\mathrm{d}x_3 \right)\mathrm{d}A \tag{16}$$

where A is the midsurface area of the sandwich panel and τ_{ij} are the components of the second Piola–Kirchhoff stress tensor.

When, as usual, only transverse distributed loads $\hat{q}_3^t$ and $\hat{q}_3^b$ over the area of the top and bottom face sheets are assumed, the variation of the work done by the external loads is given by

$$\delta W = \int_A \left(\hat{q}_3^t \delta u_3^t + \hat{q}_3^b \delta u_3^b\right)\mathrm{d}A + \int_{x_t} \left(\int_{-t^f - t^c/2}^{-t^c/2} \hat{\tau}_{n\alpha}^t \delta v_\alpha^t\,\mathrm{d}x_3 + \int_{-t^c/2}^{t^c/2} \hat{\tau}_{n3}^c \delta v_3^c\,\mathrm{d}x_3 + \int_{t^c/2}^{t^c/2+t^f} \hat{\tau}_{n\alpha}^b \delta v_\alpha^b\,\mathrm{d}x_3 \right)\mathrm{d}x_t \tag{17}$$

where x_n and x_t are the normal and tangential directions along the external boundaries of the sandwich panel. The quantities $\hat{\tau}_{ij}$ are the prescribed stress components on the boundary surfaces.

In the expression for the kinetic energy, all rotatory and tangential inertia terms are discarded. Thus, the variation of the kinetic energy takes the form

$$\int_{t^0}^{t^1} \delta T\,\mathrm{d}t = \int_{t^0}^{t^1} \int_A \left(\int_{-t^f - t^c/2}^{-t^c/2} -\rho^f \ddot{v}_3^t \delta v_3^t\,\mathrm{d}x_3 + \int_{-t^c/2}^{t^c/2} -\rho^c \ddot{v}_3^c \delta v_3^c\,\mathrm{d}x_3 + \int_{t^c/2}^{t^c/2+t^f} -\rho^f \ddot{v}_3^b \delta v_3^b\,\mathrm{d}x_3 \right)\mathrm{d}A\,\mathrm{d}t \tag{18}$$

where ρ^f and ρ^c are the mass densities of the face sheets and of the core, respectively.

The variations of the strain energy, the work by the external forces and the kinetic energy defined by Eqs. (16–18) are substituted into Hamilton's principle (15). Subsequently, the variations of the strain components are expressed in terms of the variations of the unknown displacement functions and of their spatial derivatives. For the reduction of the three-dimensional elasticity problem to an equivalent two-dimensional problem, stress resultants and the stress couples are defined as follows.

Top face sheet:

$$\left\{N_{\alpha\beta}^t, M_{\alpha\beta}^t\right\} = \int_{-t^f - t^c/2}^{-t^c/2} \tau_{\alpha\beta}^t \left\{1, \left(x_3 + \frac{t^c + t^f}{2}\right)\right\}\mathrm{d}x_3 \tag{19}$$

Bottom face sheet:

$$\left\{N_{\alpha\beta}^b, M_{\alpha\beta}^b\right\} = \int_{t^c/2}^{t^f + t^c/2} \tau_{\alpha\beta}^b \left\{1, \left(x_3 - \frac{t^c + t^f}{2}\right)\right\}\mathrm{d}x_3 \tag{20}$$

Core:

$$\left\{N^c_{i3},\, M^c_{i3}\right\} = \int_{-t^c/2}^{t^c/2} \tau^c_{i3}\{1,\, x_3\}\,\mathrm{d}x_3 \tag{21}$$

Consistent with definition (7) for the alternative face-sheet displacement functions, alternative face-sheet stress resultants and stress couples are defined as

$$\left\{N^a_{\alpha\beta},\, M^a_{\alpha\beta}\right\} = \tfrac{1}{2}\left\{\left(N^t_{\alpha\beta} + N^b_{\alpha\beta}\right),\, \left(M^t_{\alpha\beta} + M^b_{\alpha\beta}\right)\right\} \tag{22}$$

$$\left\{N^d_{\alpha\beta},\, M^d_{\alpha\beta}\right\} = \tfrac{1}{2}\left\{\left(N^t_{\alpha\beta} - N^b_{\alpha\beta}\right),\, \left(M^t_{\alpha\beta} - M^b_{\alpha\beta}\right)\right\} \tag{23}$$

With the substituting of the earlier defined expressions into the variational equation (15), the collecting of the terms corresponding to the dependence on the respective variations of the displacement functions, and the integrating by parts wherever possible, a lengthy homogeneous equation is obtained that involves the variations δu^a_i, δu^d_i, $\delta u^a_{i,\alpha}$, and $\delta u^d_{i,\alpha}$ of the displacement functions and their gradients as coefficients. Because all of these quantities are arbitrary and independent throughout A and throughout the time interval $[t^0, t^1]$, the corresponding coefficients must vanish independently. From the area integrals, the nonlinear equations of motion are obtained:

$$0 = N^a_{11,1} + N^a_{12,2} \tag{24}$$

$$0 = N^a_{12,1} + N^a_{22,2} \tag{25}$$

$$0 = N^d_{11,1} + N^d_{12,2} + (1/t^c)N^c_{13} \tag{26}$$

$$0 = N^d_{12,1} + N^d_{22,2} + (1/t^c)N^c_{23} \tag{27}$$

$$\begin{aligned} 0 = {} & \left(u^a_{3,11} + \mathring{u}^a_{3,11} + 1/r_1\right)N^a_{11} + 2\left(u^a_{3,12} + \mathring{u}^a_{3,12}\right)N^a_{12} \\ & + \left(u^a_{3,22} + \mathring{u}^a_{3,22} + 1/r_2\right)N^a_{22} + M^a_{11,11} + 2M^a_{12,12} + M^a_{22,22} \\ & + (1/t^c)\left[(t^c + t^f)/2 - u^d_3 - \mathring{u}^d_3\right]\left(N^c_{13,1} + N^c_{23,2}\right) \\ & + \left(u^d_{3,11} + \mathring{u}^d_{3,11}\right)N^d_{11} + 2\left(u^d_{3,12} + \mathring{u}^d_{3,12}\right)N^d_{12} + \left(u^d_{3,22} + \mathring{u}^d_{3,22}\right)N^d_{22} \\ & - (2/t^c)\left(u^d_{3,1} + \mathring{u}^d_{3,1}\right)N^c_{13} - (2/t^c)\left(u^d_{3,2} + \mathring{u}^d_{3,2}\right)N^c_{23} + \hat{q}^a_3 \\ & - \left(m^f + \tfrac{1}{2}m^c\right)\ddot{u}^a_3 \end{aligned} \tag{28}$$

$$\begin{aligned} 0 = {} & \left(u^a_{3,11} + \mathring{u}^a_{3,11} + 1/r_1\right)N^d_{11} + 2\left(u^a_{3,12} + \mathring{u}^a_{3,12}\right)N^d_{12} \\ & + \left(u^a_{3,22} + \mathring{u}^a_{3,22} + 1/r_2\right)N^d_{22} + M^d_{11,11} + 2M^d_{12,12} + M^d_{22,22} \\ & + \left(u^d_{3,11} + \mathring{u}^d_{3,11}\right)N^a_{11} + 2\left(u^d_{3,12} + \mathring{u}^d_{3,12}\right)N^a_{12} + \left(u^d_{3,22} + \mathring{u}^d_{3,22}\right)N^a_{22} \\ & + (2/t^c)\left(t^c/2 - u^d_3 - \mathring{u}^d_3\right)N^c_{33} + \hat{q}^d_3 - \left(m^f + \tfrac{1}{6}m^c\right)\ddot{u}^d_3 \end{aligned} \tag{29}$$

In Eqs. (28) and (29), m^c and m^f are the integrated mass densities for the core and the face sheets, respectively. Because of the adoption of the von Kármán concept, linear equilibrium conditions are obtained with respect to the tangential stress resultants $N^a_{\alpha\beta}$ and $N^d_{\alpha\beta}$, whereas the remaining two equations (28) and (29) are nonlinear.

The corresponding boundary conditions are obtained from the boundary integral. The result reads

$$u^a_n = \hat{u}^a_n \qquad \text{or} \qquad N^a_{nn} = \hat{N}^a_{nn} \tag{30}$$

$$u^a_t = \hat{u}^a_t \qquad \text{or} \qquad N^a_{nt} = \hat{N}^a_{nt} \tag{31}$$

$$u^d_n = \hat{u}^d_n \qquad \text{or} \qquad N^d_{nn} = \hat{N}^d_{nn} \tag{32}$$

$$u^d_t = \hat{u}^d_t \qquad \text{or} \qquad N^d_{nt} = \hat{N}^d_{nt} \tag{33}$$

$$u^a_3 = \hat{u}^a_3 \qquad \text{or}$$

$$\begin{aligned} & \left(u^a_{3,n} + \mathring{u}^a_{3,n}\right)N^a_{nn} + \left(u^a_{3,t} + \mathring{u}^a_{3,t}\right)N^a_{nt} + \left(u^d_{3,n} + \mathring{u}^d_{3,n}\right)N^d_{nn} \\ & \quad + \left(u^d_{3,t} + \mathring{u}^d_{3,t}\right)N^d_{nt} + M^a_{nn,n} + 2M^a_{nt,t} \\ & \quad + (1/t^c)\left[(t^c + t^f)/2 - u^d_3 - \mathring{u}^d_3\right]N^c_{n3} = \hat{M}^a_{nt,t} + \tfrac{1}{2}\hat{N}^c_{n3} \end{aligned} \tag{34}$$

$$u^d_3 = \hat{u}^d_3 \qquad \text{or}$$

$$\begin{aligned} & \left(u^a_{3,n} + \mathring{u}^a_{3,n}\right)N^d_{nn} + \left(u^a_{3,t} + \mathring{u}^a_{3,t}\right)N^d_{nt} + \left(u^d_{3,n} + \mathring{u}^d_{3,n}\right)N^a_{nn} \\ & \quad + \left(u^d_{3,t} + \mathring{u}^d_{3,t}\right)N^a_{nt} + M^d_{nn,n} + 2M^d_{nt,t} = \hat{M}^d_{nt,t} - (1/t^c)\hat{M}^c_{n3} \end{aligned} \tag{35}$$

$$u^a_{3,n} = \hat{u}^a_{3,n} \qquad \text{or} \qquad M^a_{nn} = \hat{M}^a_{nn} \tag{36}$$

$$u^d_{3,n} = \hat{u}^d_{3,n} \qquad \text{or} \qquad M^d_{nn} = \hat{M}^d_{nn} \tag{37}$$

Again, linear equations with respect to the face-sheet tangential and bending components are obtained, whereas the conditions related to the transverse displacements are nonlinear. Thus, all equations derived earlier are valid for any type of elastic or inelastic material behavior. The terms on the right-hand-side members of the boundary conditions marked by a circumflex sign are prescribed quantities. Note that within this structural model eight boundary conditions should be prescribed on each edge of the panel, and as a result, the governing equations should be of 16th order.

III. Analytical Solution for Simply Supported Elastic Panels

A. Orthotropic Linear Elastic Material

In the next developments, the special case of a simply supported rectangular panels is considered. Both the face sheets and the core are assumed to consist of an orthotropic linear elastic material. Under these conditions, an analytical treatment of the problem is possible. In this section, a brief outline of the analytical procedure will be presented.

In the case of orthotropic linear elasticity, the average stress resultants and stress couples of the face sheets are related to the average tangential and bending strains by the matrix relations

$$\begin{pmatrix} N^a_{11} \\ N^a_{22} \\ N^a_{12} \end{pmatrix} = \begin{pmatrix} A^f_{11} & A^f_{12} & 0 \\ & A^f_{22} & 0 \\ (\mathrm{sym}) & & A^f_{66} \end{pmatrix} \begin{pmatrix} \bar{\gamma}^a_{11} \\ \bar{\gamma}^a_{22} \\ 2\bar{\gamma}^a_{12} \end{pmatrix} \tag{38}$$

$$\begin{pmatrix} M^a_{11} \\ M^a_{22} \\ M^a_{12} \end{pmatrix} = \begin{pmatrix} D^f_{11} & D^f_{12} & D^f_{16} \\ & D^f_{22} & D^f_{26} \\ (\mathrm{sym}) & & D^f_{66} \end{pmatrix} \begin{pmatrix} \kappa^a_{11} \\ \kappa^a_{22} \\ 2\kappa^a_{12} \end{pmatrix} \tag{39}$$

with

$$\left\{\bar{\gamma}^a_{\alpha\beta},\, \kappa^a_{\alpha\beta}\right\} = \tfrac{1}{2}\left\{\left(\bar{\gamma}^t_{\alpha\beta} + \bar{\gamma}^b_{\alpha\beta}\right),\, \left(\kappa^t_{\alpha\beta} + \kappa^b_{\alpha\beta}\right)\right\} \tag{40}$$

$$\left(\bar{\gamma}^d_{\alpha\beta},\, \kappa^d_{\alpha\beta}\right\} = \tfrac{1}{2}\left\{\left(\bar{\gamma}^t_{\alpha\beta} - \bar{\gamma}^b_{\alpha\beta}\right),\, \left(\kappa^t_{\alpha\beta} + \kappa^b_{\alpha\beta}\right)\right\} \tag{41}$$

where $\bar{\gamma}^t_{\alpha\beta}$ and $\bar{\gamma}^b_{\alpha\beta}$ are the tangential strains of the top and bottom face sheet, respectively, whereas $\kappa^t_{\alpha\beta}$ and $\kappa^b_{\alpha\beta}$ are the corresponding bending strains. The stress resultants $N^d_{\alpha\beta}$ and $M^d_{\alpha\beta}$ are related to the tangential and bending strains $\bar{\gamma}^d_{\alpha\beta}$ and $\kappa^d_{\alpha\beta}$ of the top and bottom face sheets by relations similar to Eqs. (38) and (39).

The components of the stiffness matrices are defined in terms of the reduced stiffness matrix Q_{ij}^f of the face-sheet material by

$$\left\{A_{ij}^f, D_{ij}^f\right\} = \int_{-t^f - t^c/2}^{-t^c/2} \left(Q_{ij}^f - \frac{Q_{i3}^f Q_{j3}^f}{Q_{33}^f}\right)\left\{1, \left(x_3 + \frac{t^c + t^f}{2}\right)^2\right\} \mathrm{d}x_3 \tag{42}$$

The stress resultants N_{i3}^c and M_{i3}^c for the core are related in a similar manner to the transverse core strain measures $\bar{\gamma}_{i3}^c$ and κ_{i3}^c. The corresponding equations read

$$\begin{pmatrix} N_{33}^c \\ N_{23}^c \\ N_{13}^c \end{pmatrix} = \begin{pmatrix} A_{33}^c & 0 & 0 \\ 0 & A_{44}^c & 0 \\ 0 & 0 & A_{55}^c \end{pmatrix} \begin{pmatrix} \bar{\gamma}_{33}^c \\ 2\bar{\gamma}_{23}^c \\ 2\bar{\gamma}_{13}^c \end{pmatrix} \tag{43}$$

$$\begin{pmatrix} M_{33}^c \\ M_{23}^c \\ M_{13}^c \end{pmatrix} = \begin{pmatrix} D_{33}^c & 0 & 0 \\ 0 & D_{44}^c & 0 \\ 0 & 0 & D_{55}^c \end{pmatrix} \begin{pmatrix} \kappa_{33}^c \\ 2\kappa_{23}^c \\ 2\kappa_{13}^c \end{pmatrix} \tag{44}$$

where the stiffness components are obtained from the components Q_{ij}^c of the reduced stiffness matrix of the core material by

$$\left\{A_{ij}^c, D_{ij}^c\right\} = \int_{-t^c/2}^{t^c/2} Q_{ij}^c \left\{1, (x_3)^2\right\} \mathrm{d}x_3, \qquad i, j = 3, 4, 5 \tag{45}$$

With the constitutive equations (38), (39), (43), and (44), the equations of motion (24–29), as well as the boundary conditions (30–36), can be expressed in terms of the unknown displacement functions. Because of their intricacy, these equations are not provided here.

B. Displacement Representation

In case of a rectangular, simply supported sandwich panel, an appropriate representation for the transverse displacements is given by

$$u_3^a = w_{mn}^a \sin\left(\lambda_m^a x_1\right) \sin\left(\mu_n^a x_2\right), \qquad \lambda_m^a = m\pi/l_1, \qquad \mu_n^a = n\pi/l_2 \tag{46}$$

$$u_3^d = w_{pq}^d \sin\left(\lambda_p^d x_1\right) \sin\left(\mu_q^d x_2\right), \qquad \lambda_p^d = p\pi/l_1, \qquad \mu_q^d = q\pi/l_2 \tag{47}$$

where m, n, p, and q are the number of modal half-waves, whereas w_{mn}^a and w_{pq}^d are the unknown modal amplitudes of the transverse displacements. The quantities l_1 and l_2 are the tangential edge dimensions of the panel in the x_1 and x_2 directions, respectively.

In the assumption for the transverse displacements, Eq. (46) is related to overall buckling of the entire sandwich panel. In general, the numbers m and n of modal half-waves related to this type of instability will be equal to one or attain low integer numbers. The seond equation in the assumed form for the transverse displacements [Eq. (47)] is related to symmetric face wrinkling because it governs the difference u_3^d in the displacements of both face sheets, whereas Eq. (46) describes the average u_3^a of the transverse deflections of both face sheets. A typical face-wrinkling instability mode consists of a large number p or q of modal half-waves within the direction of the largest tangential load and a small number q or p of modal waves (in most cases a single one) in the direction perpendicular to the direction of the largest tangential stress resultant.

For the initial geometric imperfection, a form similar to the assumed form of the load-dependent transverse displacements with the same number of modal waves but different modal amplitudes is assumed:

$$\mathring{u}_3^a = \mathring{w}_{mn}^a \sin\left(\lambda_m^a x_1\right) \sin\left(\mu_n^a x_2\right) \tag{48}$$

$$\mathring{u}_3^d = \mathring{w}_{pq}^d \sin\left(\lambda_p^d x_1\right) \sin\left(\mu_q^d x_2\right) \tag{49}$$

A solution for the tangential displacement functions u_α^a and u_α^d that is consistent with the assumed transverse displacements u_3^a and u_3^d according to Eqs. (46) and (47) can be derived by the following procedure.

The first two equilibrium conditions (24) and (25) are identically satisfied by representing $N_{\alpha\beta}^a$ in terms of an Airy stress function Φ. An additional field equation for the Airy function is obtained by using the compatibility condition expressed in terms of the tangential strains $\bar{\gamma}_{\alpha\beta}^a$ of the face sheets. Substituting the tangential strains obtained from the inverse of Eq. (38) into the compatibility condition and expressing the stress resultants $N_{\alpha\beta}^a$ in terms of the Airy function yields an inhomogeneous differential equation for the Airy stress function. A general solution of this equation has been derived in a previous paper by the present authors.[20]

With this solution, explicit expressions for the stress resultants $N_{\alpha\beta}^a$ can be obtained. These expressions are consistent with the assumed form (46) and (47) for the transverse displacements. Substituting the stress resultants and the average face-sheet tangential strains $\bar{\gamma}_{\alpha\beta}^a$ into the constitutive relations (38) yields a system of two coupled differential equations for the tangential displacements u_α^a. Another system of two differential equations for the displacement functions u_α^d subsequently can be obtained by substituting the earlier determined parts of the solution into the third and fourth equilibrium conditions. Again, the solution for the tangential displacements u_α^a and u_α^d obtained from this system of equations is consistent with the assumed form (46) and (47) for the transverse displacements u_3^a and u_3^d. Thus, a consistent solution for all displacement components of the top and bottom face sheets (and thus, also for the dependent displacement components of the core) is available. This solution satisfies the first four equilibrium conditions, as well as all boundary conditions with respect to the transverse displacements and rotations identically. The remaining boundary conditions are satisfied in an integral average sense.

The only remaining unknowns are now the modal amplitudes w_{mn}^a and w_{pq}^d of the transverse displacements u_3^a and u_3^d, respectvely. These unknowns are determined by means of an extended Galerkin method. Therefore, all parts of the solution determined so far are substituted into Hamilton's principle (15). The variations of the displacement functions and their spatial derivatives are expressed through the variations of the unknown modal amplitudes, resulting in a lengthy homogeneous equation for the variations δw_{mn}^a and δw_{pq}^d. Because the variations of the modal amplitudes, again, are arbitrary and independent throughout the time interval $[t^0, t^1]$, the corresponding coefficients must vanish independently. Thus, there is a coupled nonlinear system of two equations for the two remaining unknowns w_{mn}^a and w_{pq}^d. The system is solved numerically by means of Newton's method.

IV. Results

A. Preliminaries

The sandwich shell model and the analytical solution procedure derived in Secs. II and III are now applied to an analysis of the deformation and buckling behavior structural sandwich panels. To include a variety of effects, three different types of structures are considered, all of which are simply supported along all edges. Within the first example, the case of a flat sandwich panel loaded in an in-plane compression mode with $-\hat{N}_{11}^a \neq 0$ and $-\hat{N}_{11}^d = 0$ is considered. The edges parallel to the loading direction are assumed to be freely movable with respect to the x_2 direction. Throughout the present study, the standard sign convention is adopted for the loads. Therefore, negative signs indicate compressive loads, whereas tensile loads are positive.

As a second structural example, a cylindrical sandwich shell is considered. The shell is loaded in uniaxial compression, similar to the case of the flat sandwich panel. The edges parallel to the loading direction are assumed to be immovable. The third structural example is a spherical sandwich cap with square projection, which is subjected to a transverse pressure acting on the top face sheet. In this example, all external edges are assumed to be immovable within the tangential plane.

Table 1 Face-sheet material data

Type	Material type	E_1, GPa	E_2, GPa	ν_{12}	G_{12}, GPa	Layup, deg	t^{ply}, mm
1	Carbon fiber reinforced plastic	142.0	9.8	0.34	4.3	[0/90/0]	0.125
2	Aluminum	69.0	69.0	0.3	26.5	——	0.65
3	Graphite epoxy	181.0	10.3	0.28	7.24	$[0/\pm\vartheta/90]_s$	0.25
4	Graphite epoxy	181.0	10.3	0.28	7.24	$[\pm\vartheta]_s$	0.25

Table 2 Core material data

Type	Material type	G_{13}, MPa	G_{23}, MPa	E_3, MPa	t^c, mm
1	Ciba Geigy aeroweb-type A1	60.0	35.2	298	5
2	Ciba Geigy aeroweb-type A1	26.6	15.5	109	25
3	HEXCEL 3/16-5052-0.0007	186.0	98.6	234	20
4	HEXCEL 3/16-5052-0.0007	186.0	98.6	234	40

Table 3 Plane sandwich panel buckling loads and number of modal waves

	Face sheet/core type			
Result	1/1	1/2	2/1	2/2
Type of buckling	Overall	Wrinkling	Overall	Wrinkling
Buckling load/number of modal waves $\hat{N}_{11}^a$/s, N/mm/–				
Ref. 22 (experimental)	−92.5/1	–/–	−117.0/1	–/–
Ref. 21 (analytical)	−76.0/1	−80.0/1	−121.0/1	−245.0/–
Refs. 8 and 9 (numerical)	–/–	−80.5/34	–/–	−246.0/19
Present study	−68.5/1	−84.6/35	−148.0/1	−259.0/20

Different combinations of core and face sheet materials are investigated. For the face sheets, three types of laminas consisting of carbon fiber-reinforced plastics and graphite epoxy layers with different stacking sequences, as well as the case of homogeneous aluminum face sheets, are considered. The assumed material parameters are presented in Table 1. The ply angle ϑ in all cases is counted from the x_1 axis toward the fiber direction of the respective ply. As usual, the positive direction is defined by an anticlockwise rotation about the x_3 axis. For the core layer, two types of honeycomb structures are investigated, including a Ciba Geigy aeroweb-type A1 nonmetallic honeycomb and a HEXCEL 3/16-5052-0.0007 aluminum hexagonal honeycomb structure. Both types of core material are considered in two different thicknesses. The assumed thickness and the material parameters for the different core types are given in Table 2.

B. Plane Sandwich Panel

For validation of the present analytical approach, the buckling of a flat, square sandwich panel with $l_1 = 228$ mm ($= l_2$) is investigated. Both types of aeroweb honeycomb cores and the carbon fiber-reinforced plastics, as well as the aluminum face sheet types according to Tables 2 and 1, respectively, are considered. Thus, a total number of four different sandwich panels with all possible combinations of core and face sheet types 1 and 2 are analyzed. The same configurations have been investigated both experimentally and by means of a simplified analytical approach by Pearce and Webber.[21,22] Two cases, where the face wrinkling instability is the leading failure mode, have recently been reanalyzed by Dawe and Yuan and Yuan and Dawe.[9] The results are presented in Table 3. In the present analysis, the overall instability corresponds to a deformation with $u_3^a \neq 0$, whereas face wrinkling corresponds to a deformation with $u_3^d \neq 0$ [Eqs. (46) and (47)].

Note that the present sandwich plate model in all cases predicts the correct instability modes. when the scatter in the results and some differences in the boundary conditions are considered, the correponding buckling predictions obtained by the present model are in good agreement with the experimental results by Pearce and Webber,[22] as well as with their analytical predictions,[21] and with the numerical results by Dawe and Yuan and Yuan and Dawe.[9] The advantage of the present structural model compared to the earlier ones stems from that the present model can address both the local and global instabilities at once. As a result, the present model is capable of an assessment of the local instability during the structural analysis of the entire sandwich structure and, thus, includes all possible interaction effects in a natural manner.

C. Cylindrical Sandwich Shell

As another case study, the problem of a cylindrical sandwich shell under axial compression is addressed. This problem involves interaction effects between the two different instability modes. The face sheets are assumed to consist of symmetric graphite epoxy laminas with a $[0/\pm\vartheta/90\%]_s$-deg stacking sequence (Table 1). To study the effect of the face sheet anisotropy on the overall buckling and deformation behavior, the ply angle ϑ is varied. As core material, a HEXCEL 3/16-5052-0.0007 aluminum honeycomb structure with $t^c = 20$ mm according to Table 2 is considered. A global geometric imperfection of $\mathring{w}_{mn}^a = 10$ mm is assumed to exist. No local geometric imperfection $\mathring{w}_{pq}^d$ is postulated.

In Fig. 2, the results of the investigation of the effect of the face sheet ansiotropy are presented. In the case of a ply angle $\vartheta = 60$ deg, a distinct snap-through effect is observed. The level of the applied compressive load $-\hat{N}_{11}$ first increases with increasing transverse deflection w_{mn}^a, attains a maximum followed by a decrease, before the occurrence of a secondary increase (Fig. 2a). Notice that the standard sign convention that tensile loads are positive, whereas compressive loads are negative is adopted throughout the present study.

The intensity of the snap-through jump is attenuated with the increase of the ply angle ϑ, resulting in an increased face-sheet anisotropy. At $\vartheta \approx 80$ deg, the snap-through jump is eliminated. For a ply angle $\vartheta \approx 55$ deg, the postbuckling behavior changes completely from the behavior at $\vartheta \geq 60$ deg in the sense that the direction of the transverse deflection in case of an increasing compressive load $-\hat{N}_{11}$ reverses. In addition, no snap-through effect is present in this case. A similar behavior is observed for the resulting edge load $\hat{N}_{22}$ perpendicular to the global loading direction (Fig. 2b). Note that the resulting edge load $\hat{N}_{22}$ might become tensile at sufficiently large transverse deflections w_{mn}^a of the shell center.

Slight or strong discontinuities in the slopes of both the applied edge load-deflection curve in Fig. 2a, as well as in the curve for the resulting edge load $\hat{N}_{22}$ perpendicular to the loading direction (Fig. 2b) and the resulting deflection u_1^a of the loaded edge (Fig. 2c), mark the onset of the development of the face-wrinkling instability with a nonzero difference u_3^d in the transverse deflections of both face sheets according to Eq. (47). For load levels below the respective load, no face wrinkling occurs, indicated by a vanishing modal amplitude w_{pq}^d of this type of instability (Fig. 2d). Beyond the corresponding buckling load, a face-wrinkling instability mode with a nonvanishing modal amplitude develops. In case of a global snap-through effect, for example, for a ply angle $\vartheta = 60$ deg, a temporary decrease in the modal amplitude w_{pq}^d is caused by the temporary decrease in the level of the applied compressive load $-\hat{N}_{11}$. The development of the face-wrinkling instability results in an additional increase in the displacement u_1^a of the loaded edge (Fig. 2c). Especially for $\vartheta = 55$ deg, a distinct effect consisting of a sudden increase of the modal amplitude w_{pq}^d by about 3 mm is observed. The sudden increase in the deflection u_1^a of the loaded edge results in a sudden, more or less distinct increase in the levels of both the applied compressive edge load $-\hat{N}_{11}$ as well as of the resulting compressive edge load $-\hat{N}_{22}$ perpendicular to the loading direction without a further increase in the global transverse deflection w_{mn}^a of the panel center.

Especially for a ply angle $\vartheta = 55$ deg, a strong effect is observed. Minor kinks are observed on the load-deflection curves for ply angles of $\vartheta \geq 60$ deg. In these cases, the onset of face wrinkling occurs just before the snap-through jump. Therefore, if in the considered cases the critical external load is exceeded, the snap-through effect is not only associated with a sudden increase in the overall transverse deflection u_3^a of the sandwich panel but also includes a

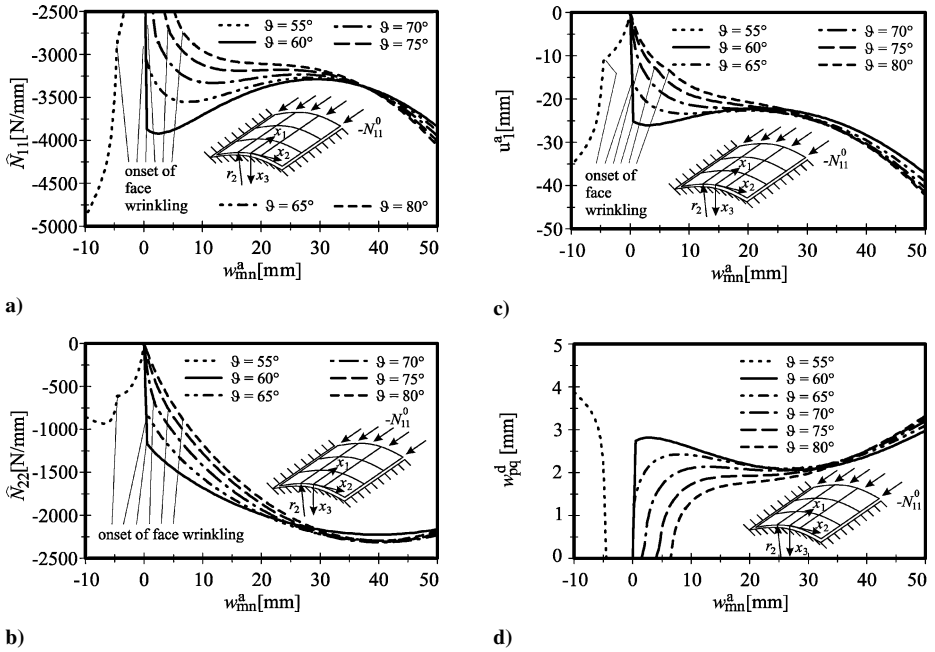

Fig. 2 Cylindrical sandwich shell: effect of face-sheet ply angle.

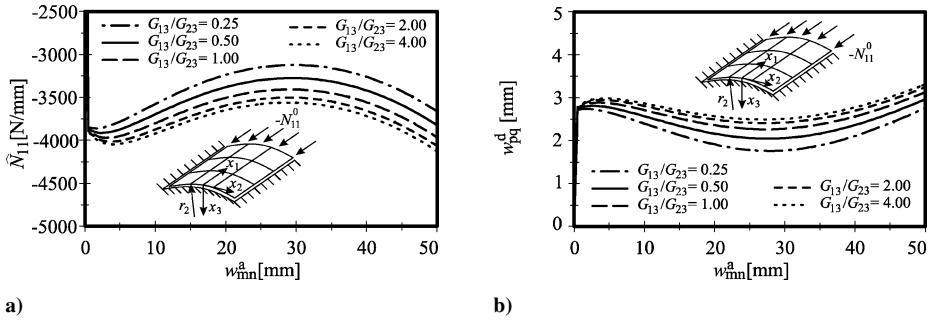

Fig. 3 Cylindrical sandwich shell: effect of transverse shear modulus.

sudden increase in the modal amplitude w_{pq}^d of the face wrinkling instability. Thus, the presence of the local face-wrinkling instability can have distinct effects on the overall load deflection and buckling behavior of sandwich panels. Notice that no such effects could be described by the classical sandwich shell models under the assumption of a transversely incompressible core.

In the previous analysis, the properties of the core have been kept constant. Because the ratio G_{13}/G_{23} of the transverse shear moduli of the core might vary for different core types, the effect of this quantity is studied next. In the underlying computations, the transverse shear modulus G_{23} is kept constant at its nominal value according to Table 2, whereas five different values of the transverse shear modulus G_{13} are considered, resulting in five different ratios G_{13}/G_{23}. The face sheet material is the same as in the earlier analyses except that the ply angle is fixed at $\vartheta = 60$ deg resulting in a distinct snap-through effect. The results are presented in Fig. 3. Observe that the variation of the transverse shear modulus G_{13} has distinct effects on the overall edge load-deflection behavior $\hat{N}_{11}(w_{mn}^a)$ (Fig. 3a), as well as on the modal amplitude w_{pq}^d of the face-wrinkling instability shown in Fig. 3b. In contrast to the effect of the ply angle ϑ considered in Fig. 2, the effects observed in the present analysis are mainly of a quantitative nature, caused by the variation of the overall core stiffness due to the variation of G_{13}. The qualitative behavior on the other hand, especially the occurrence of the snap-through effect, remains unchanged.

D. Spherical Sandwich Cap

The third structural example consists of a spherical sandwich cap of a square projection, loaded in unilateral transverse compression $\hat{q}_3^t \neq 0$. It is assumed that the core is a hexagonal HEXCEL aluminum honeycomb structure according to Table 2, type 4. Unless otherwise stated, the core thickness is $t^c = 40$ mm (case 4, Table 2). The face sheets are assumed to consist of graphite epoxy laminas with a $[\pm\vartheta]_s$ stacking sequence (face-sheet type 4, Table 1). The face-sheet ply angle ϑ is varied to study the effect of the face sheet anisotropy. All edges of the sandwich cap are assumed to be simply supported and immovable within the tangential plane with respect to the direction normal to the respective edge.

If the load $\hat{q}_3^t = 2\hat{q}_3^a$ is increased from a zero level, the deformation of the sandwich cap in conjunction with the applied boundary conditions require a shortening of the sandwich shell in both the x_1 and x_2 directions. This deformation causes the development of resulting nonzero edge loads $\hat{N}_{11}$ and $\hat{N}_{22}$, which eventually cause the development of a face wrinkling instability mode. If the transverse displacement w_{mn}^a becomes sufficiently large, the curvature of the sandwich panel in the deformed configuration changes, resulting in a subsequent decrease of the tangential shortening of the sandwich cap required by the tangential boundary conditions. The related decrease of the resulting tangential edge loads $\hat{N}_{11}$ and $\hat{N}_{22}$ eventually results in a vanishing of the face-wrinkling instability mode at a sufficiently high load level $\hat{q}_3^a$.

In Figs. 4a and 4b, the ranges in the loading and deformation evolution of the sandwich cap, in which a face wrinkling mode with a nonvanishing modal amplitude w_{pq}^d develops, are presented. Observe that the range marking the presence of a face-wrinkling instability strongly depends on the anisotropy ratio of the sandwich panel governed by the ply angle ϑ. The most narrow face-wrinkling range is obtained for the off-axes cross-ply laminate at $\vartheta = 45$ deg,

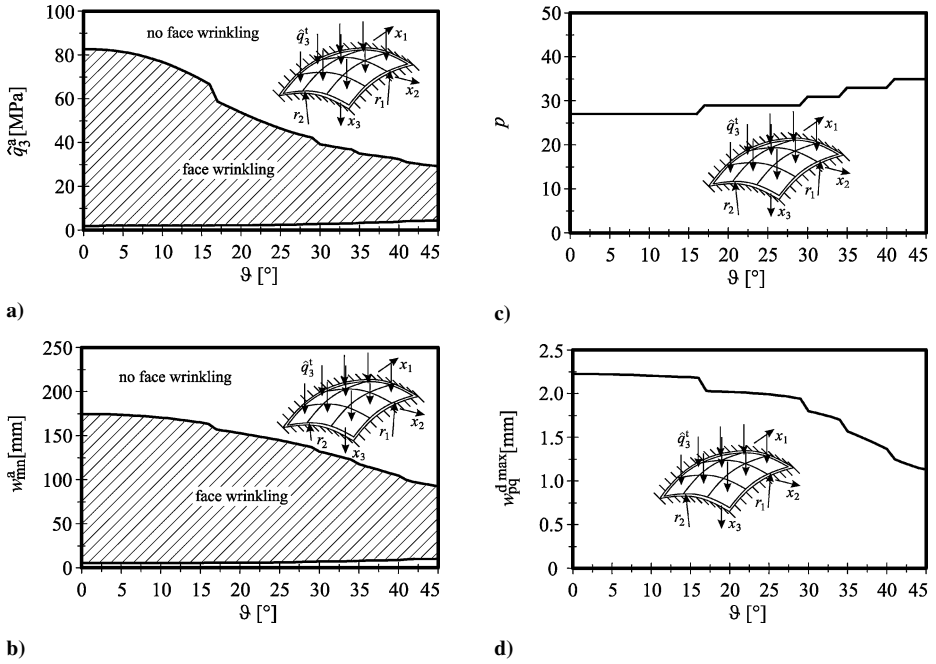

Fig. 4 Spherical sandwich cap: occurrence of face wrinkling.

where the angle between the different ply orientations is 90 deg. The anisotropy ratio of the face sheets decreases, if the ply angle is decreased. At $\vartheta = 0$ deg, the special case of a unidirectional laminate is obtained. In this case, the sandwich structure becomes rather stiff with respect to the x_1 direction, whereas a rather low stiffness is obtained perpendicular to this direction. Because the face-wrinkling mode involving the lowest overall strain energy (in the present problem) is a mode consisting of multiple modal waves in one direction (here the weak direction) and a single sine half-wave in the other direction (here the stiff direction), the resistance of the considered sandwich panel against the development of a face-wrinkling instability decreases if the face sheet ply angle approaches the case of a unidirectional laminate at $\vartheta = 0$ deg.

The observed discontinuities in the boundaries of the face-wrinkling ranges in Figs. 4a and 4b are due to the changes in the number p of modal waves. The dependence of p on the ply angle ϑ is presented in Fig. 4c. In this context, odd numbers p of modal waves in the x_1 direction involve less overall strain energy than even numbers. Therefore, no even numbers p of sine half-waves are present in any case. In addition to the global load level $\hat{q}_3^a$ and the global transverse deflection w_{mn}^a, the modal amplitude w_{pq}^d of the face-wrinkling instability mode depends on the number p of modal waves. As can be observed in Fig. 4d, the maximum modal amplitude $w_{pq}^{d\,\max}$ of the face-wrinkling instability during the loading process decreases with an increasing number p of modal waves. Because an increasing number p of modal waves at a constant maximum deflection w_{pq}^d would cause a discontinuous increase in the overall strain energy, this effect can be explained on energetic arguments.

In Figs. 5a–5d, the external load $\hat{q}_3^a$, the modal amplitude w_{pq}^d, and the resulting tangential edge loads $\hat{N}_{11}$ and $\hat{N}_{22}$, respectively, are plotted vs the global transverse deflection w_{mn}^a of the panel center. Four different ply angles ϑ are considered. Observe in Fig. 5a that the ply angle ϑ has a strong impact on the overall load-deflection behavior of the sandwich cap under consideration. Similar to the resistance against the development of the face-wrinkling instability, the overall stiffness of the sandwich cap decreases with decreasing ply angle ϑ. The dependence of the face-wrinkling resistance of the sandwich cap can again be studied in Fig. 5b, where the modal amplitude w_{pq}^d of the face-wrinkling modes is presented as a function of the global transverse deflection w_{mn}^a. With the increasing ply angle ϑ, the face wrinkling amplitude decreases in magnitude, whereas the range of a nonvanishing modal amplitude shrinks. Both effects indicate an increasing resistance of the sandwich cap against the development of a face-wrinkling instability. Note that due to a small geometric imperfection $\mathring{w}_{mn}^d$, which has to be imposed to stabilize the numerical computation, no sharp boundaries of the face wrinkling range can be obtained.

In Figs. 5c and 5d, the development of the resulting tangential edge loads $\hat{N}_{11}$ and $\hat{N}_{22}$ during the deformation process is presented. The onset and the vanishing of the face wrinkling instability result in sharp discontinuities in the slope of the curves. No such effects would have appeared in the context of a standard sandwich model involving the assumption of a transversely incompressible core. Notice that the resulting tangential edge loads become tensile at a sufficiently high transverse deflection due to the curvature change of the sandwich cap. Again, strong effects of the face-sheet anisotropy due to the variation of the ply angles are observed. Because of the anisotropy of the sandwich cap, the results for the tangential edge loads corresponding to the different spatial directions are different.

As a final analysis, the effect of the transverse elastic modulus E^c of the core is investigated. In Figs. 6a and 6b, the transverse load $\hat{q}_3^a$ and the resulting tangential edge load $\hat{N}_{11}$ for a sandwich cap with a ply angle $\vartheta = 30$ deg are presented. To study the effect of the transverse core compressibility, six different levels of the core's transverse Young's modulus are considered ranging from a rather weak core with $E_3 = 20$ MPa to a stiff core with $E_3 = 7$ GPa. All remaining core properties are kept constant at the values given in Table 2.

The modal amplitude w_{pq}^d of the face-wrinkling instability vanishes in case of the largest transverse Young's modulus, $E_3 = 7$ GPa. In this case, the face-wrinkling instability is suppressed due to the large transverse core stiffness. In all other cases, a face-wrinkling instability is present. Both the modal amplitude w_{pq}^d as well as the range where this type of instability occurs during the deformation process increase with decreasing transverse core stiffness. Because the sandwich panel becomes weaker in presence of a face-wrinkling instability, the overall load-deflection curve presented in Fig. 6a decreases with decreasing Young's modulus E_3 of the core. In Fig. 6, the direction of an increasing transvers elastic modulus E_3 is indicated by an arrow. Because the decrease of the transverse Young's modulus is related to the presence of a face-wrinkling instability with nonvanishing modal amplitude, the effect is restricted to those ranges of the deformation process where a face wrinkling mode

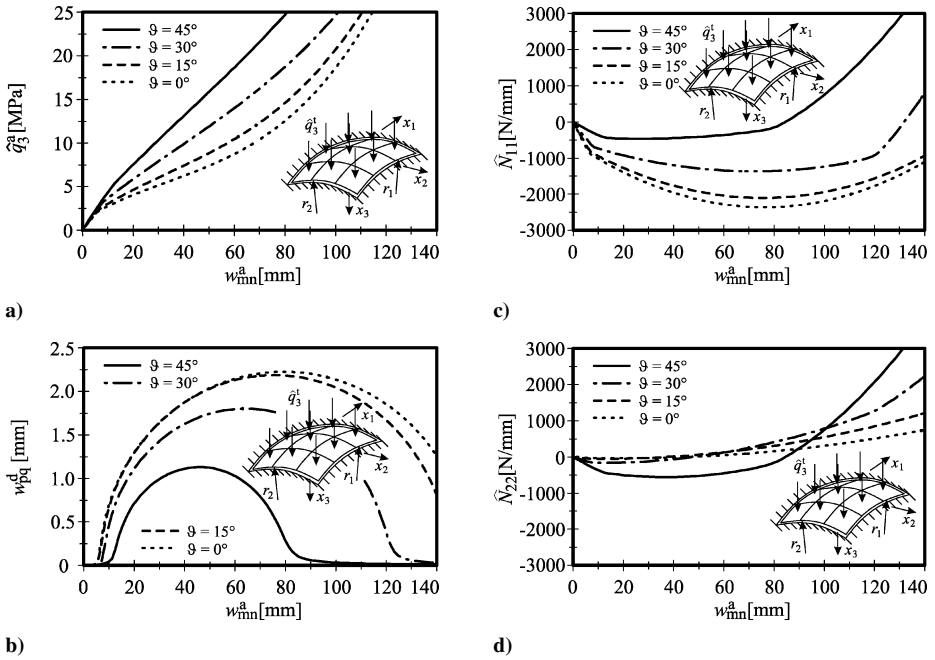

Fig. 5 Spherical sandwich cap: effect of face-sheet ply angle.

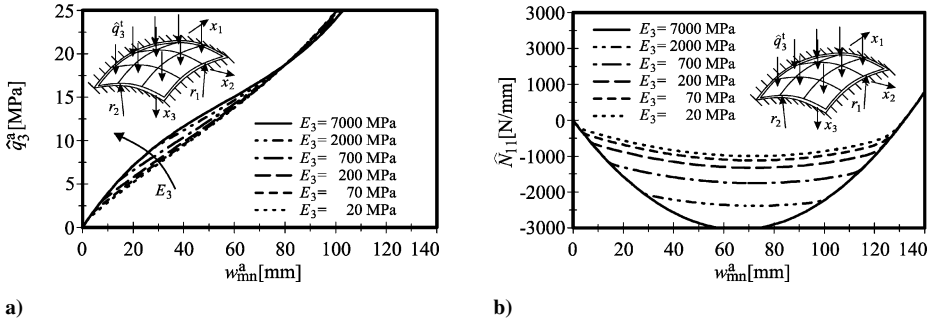

Fig. 6 Spherical sandwich cap: effect of transverse Young's modulus.

is present. Note that, for a given global load level $\hat{q}_3^a$, the overall deflection w_{mn}^a increases by up to 20% if the transverse core compressibility is considered.

The most severe effect is observed again in case of the resulting tangential edge loads $\hat{N}_{11}$ and $\hat{N}_{22}$. The resulting edge load $\hat{N}_{11}$ is plotted in Fig. 6b vs the overall deflection w_{mn}^a. In case of the stiff core with $E_3 = 7$ GPa, no face wrinkling occurs. Therefore, smooth curves $\hat{N}_{11}^a(w_{mn}^a)$ are obtained. In all other cases, kinks mark the onset and the vanishing of the face-wrinkling instability. In both cases, strong effects of the transverse elastic modulus E_3 of the core on the magnitude of the resulting edge loads $\hat{N}_{11}$ are observed. In this context, the level of the compressive edge load $-\hat{N}_{11}$ decreases. These results again indicate that the transverse core compressibility and the related local face-wrinkling instability might have significant effects on the overall deformation behavior of structural sandwich panels.

V. Conclusions

The present study is concerned with a comprehensive analysis of doubly curved anisotropic sandwich shells with weak cores including all principal effects especially in the postbuckling range. To capture the effect of the transverse core compressibility, a higher-order multilayer shell theory is developed. In addition, the structural model accounts for geometric nonlinearity, initial geometric imperfections, and inertia effects. The local face-wrinkling instability can be addressed during the structural analysis rather than during a postprocessing as in the previous models available in the literature. Thus, the interaction of the face-wrinkling instability with the global buckling as well as external geometry and curvature effects or effects of the external geometry and the loading conditions on the face-wrinkling mode are addressed in a natural manner.

The model is applied to the analysis of different cases of simply supported sandwich panels with laminated face sheets and orthotropic core. Both flat as well as curved sandwich panels are considered. Based on an extended Galerkin procedure, an analytical solution is obtained. The model is validated against available experimental results, as well as against alternative analytical and numerical results presented by other authors. The model proposed in the present study proves to be both accurate and numerically efficient.

Two structural examples involving the postbuckling behavior of a cylindrical sandwich panel under axial compression and with the deformation behavior of a spherical sandwich panel under transverse normal pressure are considered. In both examples, distinct effects of the local face-wrinkling instability on the overall deformation and postbuckling behavior of the entire structures are observed. Because the local face-wrinkling instability is closely related to the transverse compressibility of the core, the classical sandwich shell models with transversely incompressible core would provide inadvert predictions.

Strong effects of the face sheet anisotropy on the development of the different local and global buckling modes are observed. In this context, the snap-through effect in the postbuckling of the geometrically imperfect cylindrical sandwich shell under axial compression can be eliminated by an appropriate choice of the face-sheet stacking sequence with appropriate ply angles. The additional shortening of the sandwich panel during the development of the face-wrinkling instability has distinct effects on the overall load-deflection behavior, especially in case of the resulting tangential edge loads. A similar

effect is observed in the example of the spherical sandwich cap under transverse pressure where the occurrence of the face-wrinkling instability mode results in a decrease of the overall panel stiffness and, thus, in a decrease of the external loads required for a specific deformation. The development of the face-wrinkling instability depends on the anisotropy induced by varying the ply angles of the laminated face sheets.

Thus, the deformation and buckling behavior of structural sandwich panels involve complex effects of the core and face-sheet anisotropy. The present refined sandwich shell theory enables a comprehensive analysis of structural sandwich shells including all major features. Especially the effects of the external geometry, the effects of loading and boundary conditions on the development of the face-wrinkling instability, and the effects of the face-wrinkling instability on the overall load deflection behavior, as well as interaction effects, can be analyzed. Because of their nonlinear nature, these effects cannot adequately be addressed in classical decoupled approaches. Finally, the high numerical efficiency of the analytical solution procedure based on the extended Galerkin method should be emphasized.

Acknowledgments

This work has been financially supported by the Office of Naval Research (Composites Program) under Grant N00014-02-1-0594. The financial support and the interest and encouragement of the Grant Monitor, Y. D. S. Rajapakse, are gratefully acknowledged. The authors express their thanks to the anonymous reviewer for valuable comments to improve the paper.

References

[1]Skvortsov, V., and Bozhevolnaya, E., "Two-Dimensional Analysis of Shallow Sandwich Panels," *Composite Structures*, Vol. 53, 2001, pp. 43–53.

[2]Ferreira, J. M., Barbosa, J. T., Torres Marques, A., and César de Sá, J., "Non-Linear Analysis of Sandwich Shells: The Effect of Core Plasticity," *Computers and Structures*, Vol. 76, 2000, pp. 337–346.

[3]Barut, A., Madenci, E., Heinrich, J., and Tessler, A., "Analysis of Thick Sandwich Construction by a {3, 2}-Order Theory," *International Journal of Solids and Structures*, Vol. 38, 2001, pp. 6063–6077.

[4]Allen, H. G., *Analysis and Design of Structural Sandwich Panels*, Pergamon, Oxford, 1969.

[5]Frostig, Y., Baruch, M., Vilnay, O., and Sheiman, I., "High-Order Buckling Theory for Sandwich-Beam Behavior with Transversely Flexible Core," *Journal of Engineering Mechanics*, Vol. 118, 1992, pp. 1026–1043.

[6]Bozhevolnaya, E., and Frostig, Y., "Nonlinear Closed-Form High-Order Analysis of Curved Sandwich Panels," *Composite Structures*, Vol. 38, 1997, pp. 383–394.

[7]Frostig, Y., "Buckling of Sandwich Panels with a Flexible Core—High-Order Theory," *International Journal of Solids and Structures*, Vol. 35, 1998, pp. 183–204.

[8]Dawe, D. J., and Yuan, W. X., "Overall and Local Buckling of Sandwich Plates with Laminated Faceplates, Part I: Analysis," *Computer Methods in Applied Mechanics and Engineering*, Vol. 190, 2001, pp. 5197–5213.

[9]Yuan, W. X., and Dawe, D. J., "Overall and Local Buckling of Sandwich Plates with Laminated Faceplates, Part II: Applications," *Computer Methods in Applied Mechanics and Engineering*, Vol. 190, 2001, pp. 5215–5231.

[10]Pai, P. F., and Palazotto, A. N., "A Higher-Order Sandwich Plate Theory Accounting for 3-D Stresses," *International Journal of Solids and Structures*, Vol. 38, 2001, pp. 5045–5062.

[11]Librescu, L., Hause, C., and Camarda, C. J., "Geometrically Nonlinear Theory of Initially Imperfect Sandwich Curved Panels Incorporating Nonclassical Effects," *AIAA Journal*, Vol. 35, 1997, pp. 1393–1403.

[12]Vonach, W. K., and Rammerstorfer, F. G., "A General Approach to the Wrinkling Instability of Sandwich Plates," *Structural Engineering and Mechanics*, Vol. 12, 2001, pp. 363–376.

[13]Librescu, L., and Hause, T., "Recent Developments in the Modeling and Behavior of Advanced Sandwich Constructions: A Survey," *Composite Structures*, Vol. 48, 2000, pp. 1–17.

[14]Noor, A. K., Burton, W. S., and Bert, C. W., "Computational Models for Sandwich Panels and Shells," *Applied Mechanics Reviews*, Vol. 49, 1996, pp. 155–199.

[15]Vinson, J. R., "Sandwich Structures," *Applied Mechanics Reviews*, Vol. 54, 2001, pp. 201–214.

[16]Starlinger, A., and Rammerstorfer, F. G., "A Finite Element Formulation for Sandwich Shells Accounting for Local Failure Phenomena," *Sandwich Construction 2, Proceedings of the Second International Conference on Sandwich Construction*, EMAS Publishing, Warley, England, U.K., 1992, pp. 161–179.

[17]da Silva, L. A. P. S., and Santos, J. M. C., "Localised Formulations for Thick "Sandwich" Laminated and Composite Structures," *Computational Mechanics*, Vol. 22, 1998, pp. 211–224.

[18]Wadee, M. A., and Hunt, G. W., "Interactively Induced Localized Buckling in Sandwich Structures with Core Orthotropy," *Journal of Applied Mechanics*, Vol. 65, 1998, pp. 523–528.

[19]Hohe, J., and Librescu, L., "A Comprehensive Nonlinear Model for Sandwich-Shells with Anisotropic Faces and Compressible Core," AIAA Paper 2002-1245, April 2002.

[20]Hohe, J., and Librescu, L., "A Nonlinear Theory for Doubly Curved Anisotropic Sandwich Shells with Transversely Compressible Core," *International Journal of Solids and Structures*, Vol. 40, 2003, pp. 1059–1088.

[21]Pearce, T. R. A., and Webber, J. P. H., "Buckling of Sandwich Panels with Laminated Face Plates," *Aeronautical Quarterly*, Vol. 23, 1972, pp. 148–160.

[22]Pearce, T. R. A., and Webber, J. P. H., "Experimental Buckling Loads of Sandwich Panels with Carbon Fibre Face Plates," *Aeronautical Quarterly*, Vol. 24, 1973, pp. 295–312.

A. Palazotto
Associate Editor